# Chapter 9

# Summary

## 9.1 Equilibrium states

Equilibrium states are exact solutions of the equations of motion with all occurrences of the time derivative $\partial/\partial t$ set to zero. The momentum equation (1.6.5) therefore reduces to a statement that the sum of forces must be everywhere zero.

We have assumed that, if the equilibrium state involves a nonzero current, that current will be directed in one and only one of the coordinate directions[1]. Such a unidirectional current can be incompressible (see 1.6.2) only if its speed does not vary in the direction of flow. In Cartesian coordinates, this invariance of the equilibrium flow implies that the self-advection term in the momentum equation (1.6.4, 1.6.1) must vanish:

$$[\vec{u} \cdot \vec{\nabla}]\vec{u} = 0. \tag{9.1.1}$$

The single exception to (9.1.1) is circular flow in cylindrical coordinates (chapter 4), where the self-advection term is not zero but instead contributes the centrifugal force.

Each of the force terms can be neglected under certain plausible assumptions, with the exception of the pressure gradient. The gravitational term can be zero either in a zero-gravity environment where $g = 0$ or in a fluid with constant density such that $b = 0$. The viscous term can be zero if the fluid is assumed to be inviscid $\nu = 0$ or if the flow is such that the Laplacian of the velocity field is everywhere zero. The same is true of the diffusion term in the buoyancy equation. The Coriolis term can be zero in a non-rotating environment ($f = 0$) or in a state of no motion. The centrifugal force vanishes in a parallel flow.

In each of the equilibria considered here, most (or all) of these "optional" force terms are zero, and that the pressure field is arranged so as to balance whichever force terms are active. We can therefore classify equilibria in terms of the force that the pressure gradient must balance (see table 9.1).

[1] We have found ways to accommodate some other classes of flow, e.g. veering flows (section 5.5) and flows that are not quite in equilibrium (sections 6.2 and 7.1.3).

| force | equilibrium | chapter(s) |
|---|---|---|
| none | | 3 |
| gravity | hydrostatic | 2, 5, 8 |
| viscosity | frictional | 6, 7 |
| Coriolis | geostrophic | 8 |
| centrifugal | cyclostrophic | 4 |

**Table 9.1:** Summary of equilibrium states.

## 9.2 Instabilities

### 9.2.1 Mechanisms

The mechanism of convective instability is intuitively simple: gravity drives vertical accelerations that must overcome the damping effects of viscosity and diffusion.

Shear and baroclinic instabilities are understood in terms of wave resonances: vortical waves in the case of parallel shear flow (section 3.13); Eady waves in the case of baroclinic instability.

### 9.2.2 Rules of thumb

Table 9.2 gives some properties of stability boundaries and fastest-growing instabilities in the simplest more-or-less accurate form. See the chapter listed for details.

| instability | wavelength | growth rate | criterion | chapter |
|---|---|---|---|---|
| convection | $2.8H^{**}$ | | $Ra > 657.5$ | 2 |
| shear layer: $U = u_0 \tanh \frac{z}{h}$ | $7 \times 2h$ | $0.2\ \frac{u_0}{h}$ | inflection point | 3 |
| jet (sinuous mode): $U = u_0\ \mathrm{sech}^2 \frac{z}{h}$ | $3.5 \times 2h$ | $0.16\ \frac{u_0}{h}$ | inflection point | 3 |
| stratified shear flows (all) | | | $Ri_{min} < 1/4$ | 5 |
| vortex (barotropic) | | | inflection point | 4 |
| vortex (axisymmetric) | | | $\Phi_{min} < 0$ | 4 |
| plane Poiseuille flow: $U = 4u_0 \frac{z}{h}\left(1 - \frac{z}{h}\right)$ | $3h^{**}$ | | $Re > 11600$ | 6 |
| symmetric: $U = U_y y + U_z z$ | none | $\lvert f \rvert \sqrt{\frac{1}{Ri} - \frac{f_a}{f}}$ | $Ri < \frac{f_a}{f}$ | 8 |
| baroclinic (Eady): $U = U_z z$ | $\frac{3.9}{P} H$ | $0.3 \frac{\lvert f \rvert}{\sqrt{Ri}}$ | | 8 |

**Table 9.2:** Rules of thumb. Double asterisks $^{**}$ indicate that the wavelength pertains to the critical state. Otherwise it is the wavelength of the fastest-growing mode.

### 9.2.3 Numerical methods

We have explored the simplest numerical approach to computing the evolution of perturbations: a matrix method based on low-order finite differences. Boundary conditions are based on various assumptions, e.g.

- Boundaries are impermeable, i.e. the perpendicular component of the velocity vanishes.
- Boundaries are frictionless, allowing no viscous flux of momentum.
- Boundaries are rigid, i.e. all components of velocity vanish.
- Boundaries maintain constant temperature (or buoyancy).
- Boundaries are insulating, i.e. allowing no flux of buoyancy.

We have also explored the use of asymptotic boundary conditions to approximate an infinite domain.

The matrix method can be refined in several ways:

- Higher-order finite differences are an obvious extension of the present method.
- Compact differences may offer a major increase in accuracy at the cost of a great deal more algebra and coding. Derivatives are approximated using an implicit formulation, e.g.

  $$\alpha f'_{i-1} + \beta f'_i + \gamma f'_{i+1} = A f_{i-1} + B f'_i + C f_{i+1}.$$

  The constants $\alpha, \beta, \gamma, A, B$ and $C$ are determined using Taylor series just as in sections 1.5.2 and 1.5.3.
- Stability equations can also be discretized using Fourier series or other sets of orthogonal basis functions. In that case, the eigenvector contains not function values at grid points but rather Fourier coefficients, e.g. the $w_n$'s in

  $$\hat{w} = \Sigma_n w_n e^{i\mu_n z}.$$

  In this case the derivative matrices are very simple, e.g.:

  $$D_{mn} = i\mu_n I_{mn}$$

An entirely different approach is the *shooting method* (e.g. Hazel 1972). A stability equation such as the Rayleigh equation is solved as an initial value problem starting at one boundary and ending at the other. The initial conditions for the integration are based on the boundary condition, and parameter values (e.g. $k, \sigma$ are guessed. One then repeats the integration with successively refined parameter values until the second boundary condition is satisfied. Shooting methods are generally more complicated to code than matrix methods, but they are faster for the same level of accuracy, and they allow more flexibility in the choice of boundary conditions. The main drawback is that one can never be certain that all unstable modes have been found.

## 9.3 References

Hazel, P., 1972: "Numerical studies of the stability of inviscid stratified shear flows." *Journal of Fluid Mechanics*, **51**, 39-61.

# Chapter 10

# A look ahead: instability and turbulence

The relationship between instability and turbulence is complex. To take advantage of the relative simplicity of linear instability theory, we must understand that relationship much better than we do today. One approach is to relax the assumption of small-amplitude perturbations by numerically solving the fully nonlinear equations. This reveals a sequence of instabilities that lead to turbulence (section 10.1), each of which we can try to understand through a similar analysis.

In observational science, we find that nature rarely cooperates in creating the simple, idealized scenarios that our equations and theorems can describe. Instead, we must take a step back and look at turbulence from a less rigorous, yet intuitively appealing, perspective (section 10.2).

## 10.1 Secondary instabilities and the transition to turbulence

What happens after an unstable mode begins to grow? At some point it becomes large enough that the linearization becomes invalid. Exponential growth is damped. Beyond this time, the disturbance may simply decay, or it may exhibit a secondary instability. Analysis of this evolution is extremely difficult, and is best done using a direct numerical simulation (DNS) of the fully nonlinear equations (section 1.6).

Figure 10.1 shows a sequence of snapshots from DNS of a stratified shear layer. Initially, the minimum Richardson number was 0.08, so the Miles-Howard instability criterion was easily satisfied. The horizontal boundaries are periodic, with domain length chosen to accommodate two wavelengths of the fastest-growing mode. In the first snapshot (figure 10.1a), the fastest-growing mode has grown to form a sequence of billows (compare with figure 5.1, for example). Within each billow is a region where dense fluid overlies buoyant fluid, inviting convective instability.

The next stage is the growth of a subharmonic instability which causes adjacent billows to pair. The result appears as a single large billow straddling the edge of the domain (figure 10.1b). This instability is essentially a manifestation of the primary instability with wavenumber equal to half that of the fastest growing mode. Although its growth rate is relatively small, its large wavelength allows it to grow more-or-less independently of the fastest-growing mode, and when it reaches large amplitude it simply swallows up the original billows. If $Ri$ is small enough, this process can occur repeatedly as successively larger modes reach finite amplitude. This is an example of an upscale energy cascade.

Within the merging billows, we see a row of four convection cells resulting from the overturning noted

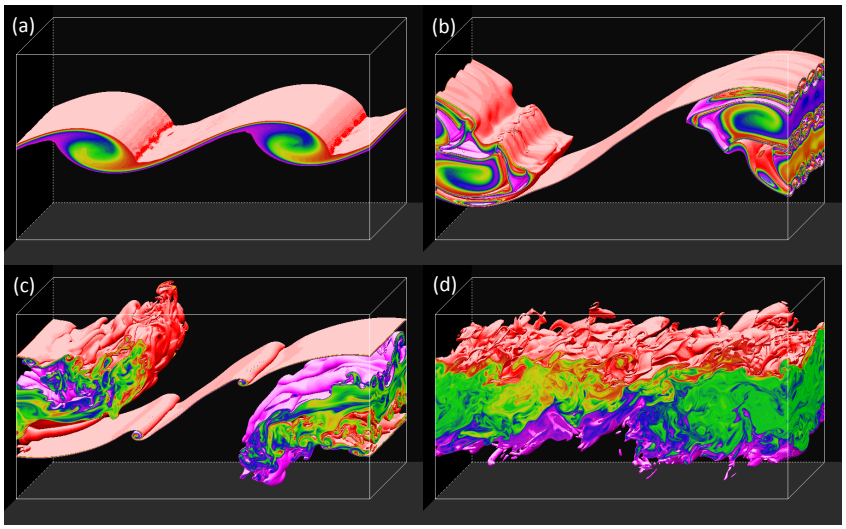


**Figure 10.1:** Snapshots of the buoyancy field from a nonlinear simulation of an unstable shear layer as it becomes turbulent. (a) Kelvin-Helmholtz instability. (b) Subharmonic pairing instability, convective instability. (c) Secondary KH instability. (d) Turbulence. Parameter values $Ri_b = 0.08$, $Re = 800$, $Pr = 7$. Horizontal boundaries are periodic. Colors range from -0.6$b_0$ to +0.6$b_0$; values outside this range are transparent. For further details see section 10.4 or Smyth and Thorpe (2012).

earlier. Note that the cells are oriented in the direction of the mean flow, as predicted by stability theory (homework #7). This secondary instability grows very quickly, leading to the development of turbulence within the core of the merged billow (figure 10.1c).

In the center of the domain, the strain between the large billows creates a region of intense strain which compresses the transition layer to form a sharp gradient of buoyancy and velocity. If the gradient Richardson number in that thin layer is small enough, secondary KH billows develop. The secondary convective and KH instabilities are examples of a downscale energy cascade. The ultimate result of the cascade is that the entire structure breaks down into turbulence (figure 10.1d).

This is only one possible evolution of a stratified shear layer. With different values of $Ri_b$, $Re$ and $Pr$, different sequences of secondary instabilities are found.

## 10.2 Marginal instability

In linear instability theory, we assume that at some initial time the flow takes a very simple, laminar, equilibrium form which is then perturbed, and we compute the initial growth of the perturbation. In real geophysical fluids this chain of events is rarely found. Instabilities observed in nature grow in environments that are already turbulent thanks to previous instabilities. At finite amplitude, instabilities break and generate turbulence whose ultimate effect is to return the mean flow towards a new stable state.

The hypothesis of marginal instability suggests that a flow can remain in a state of approximate equilibrium through the combined action of external forcing, which tends to destabilize the flow, and sporadic instabilities. A nice analogy was proposed by Bak et al. (1988): a sandpile is continually steepened by the addition

**Figure 10.2:** A marginally stable, forced-dissipative system (www.complexityacademy.io). The angle of repose is maintained, on average, by random, small avalanches.

of more sand, but if the slope becomes too steep, an avalanche will form, reducing the slope. Through the action of many, sporadic avalanches, the slope is maintained, on average, at the angle of repose (figure 10.2). That angle depends on the grade of the sand.

Called "self-organized criticality", this behavior is characteristic of many so-called "forced-dissipative" systems. Examples include earthquakes and forest fires (Jensen 1998). In the case of geophysical turbulence, we imagine that some external force such as wind or solar heating acts continually to destabilize the fluid while sporadic turbulent events relieve the instability.

Figure 10.3 shows an example from the eastern equatorial Pacific. The trade winds blow the surface water to the west, generating the south equatorial current (SEC, figure 10.3a). These pile up against the Asian coastlines, and the weight of that extra water increases the subsurface pressure. The resulting pressure gradient drives a return flow at depth called the equatorial undercurrent (EUC).

Shear and stratification both increase to maxima just above the EUC core (figure 10.3b). Their ratio, $Ri$, is remarkably uniform over much of this depth range, and is conspicuously close to the critical value 1/4 (figure 10.3c). We'll have more to say about this.

A useful measure of turbulence intensity is the rate at which its kinetic energy is dissipated by viscosity, usually denoted $\varepsilon$.[1] Turbulence remains strong down to 80m depth. Because this turbulence coexists with strong stratification, the turbulence is doing a lot of work against gravity by exchanging warm, buoyant water from the surface mixed layer with cold water from the thermocline. The result is that this region is the global maximum of heat uptake by the ocean.

Now as for the Richardson number being "conspicuously close" to 1/4. What is happening (figure 10.4) is that forcing from the trade winds acts continuously to increase the shear, and therefore to decrease $Ri$. But whenever $Ri$ drops below 1/4, instability generates turbulence which mixes out the shear, thereby increasing $Ri$ to values >1/4. The ultimate result is that $Ri$ fluctuates more-or-less randomly around 1/4.

## 10.3 References

Bak, P., C. Tang, and K. Wiesenfeld, 1987: "Self-organized criticality: an explanation of the $1/f$ noise." *Phys. Rev. Lett.* **59**, 381.

Jensen, H.J. 1998: *Self-organized criticality: emergent complex behavior in physical and biological systems.*, Cambridge University Press.

Smyth, W.D. and J.N. Moum, 2013: "Marginal instability and deep cycle turbulence in the eastern equatorial

[1] Not to be confused with the expansion parameter.

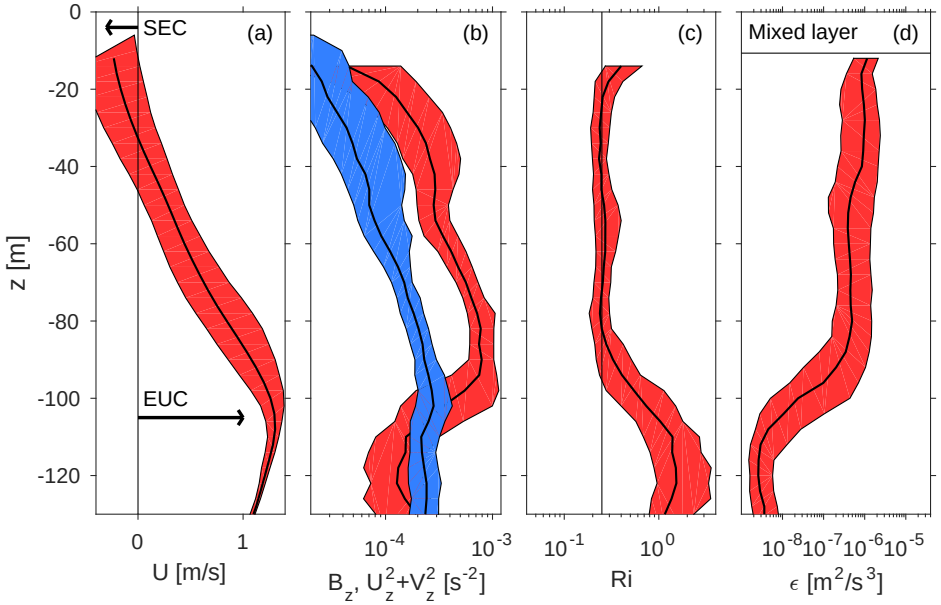


**Figure 10.3:** Mean flow and turbulence in the upper equatorial Pacific. Two weeks of shipboard observations were taken on the equator at 140W in October, 2008. Profiles show the median and the quartile range at each depth. (a) Zonal velocity, showing the South Equatorial Current and the Equatorial Undercurrent. (b) Buoyancy gradient $B_z$ (blue) and squared shear (red). (c) Gradient Richardson number. (d) Turbulent kinetic energy dissipation rate. See Smyth and Moum (2013) for further details.

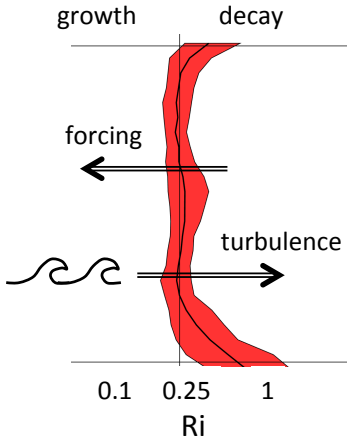


**Figure 10.4:** Schematic of processes acting in the state of marginal instability. Red area shows a Richardson number profile from the upper equatorial Pacific (similar to figure 10.3c.)

Pacific ocean", *Geophys. Res. Lett.* **40**, 1âĂŞ5.

———— and S.A. Thorpe, 2012: "Glider measurements of overturning in a Kelvin-Helmholtz billow train", *J. Mar. Res.* **70**, 119-140.

## 10.4 Appendix: details of the nonlinear simulation

The simulated mixing event employed here is a numerical solution of the Navier-Stokes equations in the Boussinesq approximation (1.6) for a non-rotating environment $f = 0$. Boundary conditions are periodic in the horizontal directions, and free-slip and insulating in the vertical. The molecular properties of the modeled fluid are consistent with thermally inhomogeneous water. The kinematic viscosity $\nu$ is $1.0 \times 10^{-6}\mathrm{m}^2\mathrm{s}^{-1}$ and the diffusivity $\kappa$ is $1.4 \times 10^{-7}\mathrm{m}^2\mathrm{s}^{-1}$, so that the Prandtl number is 7.

Initial mean profiles of streamwise velocity and density are chosen to represent a stratified shear layer:

$$\frac{U(z)}{u_0} = -\frac{B(z)}{b_0} = \tanh\frac{z}{h}$$

with half-changes $b_0 = 1.6 \times 10^{-5}$ m s$^{-2}$ in buoyancy and $u_0 = 5.3 \times 10^{-3}$m s$^{-1}$ in velocity, and half-thickness $h = 0.15$m. A small perturbation is added to excite primary and secondary instabilities. The minimum Richardson number is $Ri_b$ is 0.08 and the initial Reynolds number $Re$ is 800.

Domain dimensions are $4.19 \times 0.87 \times 2.18$m. The domain is designed to accommodate two wavelengths of the primary Kelvin-Helmholtz instability[2] and four of the secondary convective instability. Upper and lower boundaries are impermeable, frictionless and constant buoyancy. They are placed well above and below the shear layer to minimize their impact on the flow.

[2]The shear layer thickness is $2h = 0.30m$. According to the rule of thumb for shear instability, the wavelength is 7 times this, 2.1m, and the domain length is twice that wavelength.